XLI CILAMCE
XLI Ibero-Latin American Congress on Computational Methods in Engineering
16-19 November, 2020 FOZ DO IGUAÇU PARANÁ - BRAZIL

Experimental and Finite Element Analysis of Pullout Test on GFRP Rebars

Luis Henrique Pereira França[1], Francisco Estevão Damasceno Filho[1], Marcelo Silva Medeiros Júnior[1], Antônio Eduardo Bezerra Cabral[1]

[1]*Dept. Structural Engineering and Civil Construction, Federal University of Ceará*
Campus do Pici - Bloco 728, 60440-900, Fortaleza/Ceará, Brazil
luishenriquelhpf@gmail.com, damascenoestevao@alu.ufc.br, marcelomedeiros@ufc.br, eduardo.cabral@ufc.br

Abstract. Rebars with fiber glass reinforced polymer (GFRP) are a viable option in highly aggressive environments. They also make the structure lighter, more sustainable and have high corrosion resistance. In this article, an experimental program was carried out to verify the maximum pullout force, in addition to a numerical analysis and computational simulation. The finite element method was used for the computational simulation of concrete reinforced with GFRP. A constant tractive force was applied at the end of the rebar, from which the strain and maximum principal stresses were analyzed. The displacements and concrete-GFRP adhesion were verified through the Hertz contact theory and Coloumb friction theory, in the ABAQUS software. The results showed that the incorporation of epoxy resin had little influence on the pullout force. The experimental and numerical analysis showed an increase of about 20% in the pullout force of the GFRP bars, although this should not be the only limiting factor for the use of GFRP rebars in civil construction.

Keywords: GFRP, pullout, ABAQUS, finite elements, concrete.

1 Introduction

Glass fiber reinforced polymers (GFRP) are materials with applicability mainly in aggressive environments, either as reinforcement or incorporation in civil infrastructure [1–3]. Fiber-reinforced polymers (FRP) are a viable option in the process of structural reinforcement and rehabilitation, when durability, lightness and corrosion resistance are also taken into account, along with strength.

It is recommended to use FRP mainly in highly aggressive environments, such as sewage and water treatment plants, marine environments, oil platforms, among others [2, 4, 5]. The union of reinforcements with steel bars can happen through three mechanisms, chemical connection, mechanical characteristics and the aggregate [5]. For the GFRP, the main mechanisms that guarantee the FRP-concrete adhesion are the properties of the fibers, the resin matrix, and the contact surface [4, 6, 7].

Just as concrete has an interface zone, FRP bars have a transition zone between resin and rebar fibers. GFRP bars have low modulus of elasticity, so this transition zone is one of the main factors to be considered in the pullout force. Fibers with a high modulus of elasticity (carbon and aramid) have less strength at the FRP-concrete interface, consequently a premature failure may occur due to shear stress.

This study compared pullout strength of GFRP and steel bars, and the influence of resin on the contact surface, through pullout tests. The results served as basis for recommendations on the use of GFRP in structural reinforcement and incorporation in construction.

2 Literature review

2.1 Coulomb's Law

The relative movement between two bodies will occur if the tangential force (F_t) is greater than the normal force (F_N) multiplied by the coefficient μ. Considering static friction, there is no slipping between the bodies, according to eq. (1). For this to happen, the relative speed between the bodies must be zero.

$$|F_t| < \mu |F_N|. \tag{1}$$

According to eq. (2), when considering equality, there might be slipping between the bodies. Being $\dot{u}^1$ and $\dot{u}^2$ are velocity.

$$|F_t| = \mu |F_N| \rightarrow |(\dot{u}^{(2)} - \dot{u}^{(1)})|T \geq 0. \tag{2}$$

Slip conditions can be explained by eq. (3), which does not consider slip, and eq. (4), which considers slip between the bodies.

$$|F_t| = \mu |F_N| < 0 \rightarrow \dot{u}^{(1)} = \dot{u}^{(2)}, \tag{3}$$

$$|F_t| = \mu |F_N| < 0 \rightarrow |(\dot{u}^{(2)} - \dot{u}^{(1)})| \geq 0. \tag{4}$$

2.2 Hertz contact

The contact region is formed by the junction of two regions, their intersection is formed by two points (P_1,P_2), which are susceptible to displacements ($\bar{u}_{z1}$, $\bar{u}_{z2}$). The points will be in contact if the sum of the strains is equal to the sum of the displacements, as shown in eq. (5).

$$\delta_1 + \delta_2 = \bar{u}_{z1} + \bar{u}_{z2}. \tag{5}$$

According to eq. (6), the bodies will not be in contact if, where δ_1 and δ_2 are strains between bodies.

$$\delta_1 + \delta_2 < \bar{u}_{z1} + \bar{u}_{z2}. \tag{6}$$

In Hertz hypothesis, the surfaces are continuous, the strains are small, the contact area is small, there is no friction between the surfaces in contact [8, 9]. The eccentricity (e) and the curvature (k) are calculated by eqs. (7) and (8) respectively, in which 'a' is a small semi axis, and 'b', the longest axis.

$$e^2 = 1 - k^2. \tag{7}$$

$$k = \frac{b}{a}. \tag{8}$$

According to eqs. (9) and (10), it is possible to obtain the effective mean radius of curvature (R_m) and equivalent radius of curvature (R_e), respectively. Where A and B are constant. A and B are constants, and are calculated by eqs. (11) and (12). Where R_{1x}, R_{2x},R_{1y} and, R_{2y} are half-shaft radius.

$$R_m = \frac{1}{A + B}, \tag{9}$$

$$R_e = \left(\frac{1}{2}\right)(AB)^{-\frac{1}{2}}. \tag{10}$$

$$(A+B) = \frac{1}{2}\left(\frac{1}{R_{1x}} + \frac{1}{R_{1y}} + \frac{1}{R_{2x}} + \frac{1}{R_{2y}}\right), \tag{11}$$

$$(B-A) = \frac{1}{2}\left(\left(\frac{1}{R_{1x}} - \frac{1}{R_{1y}}\right)^2 + \left(\frac{1}{R_{2x}} - \frac{1}{R_{2y}}\right)^2 + 2\left(\frac{1}{R_{1x}} - \frac{1}{R_{1y}}\right)\left(\frac{1}{R_{2x}} - \frac{1}{R_{2y}}\right)cos(2\alpha)\right)^{\frac{1}{2}}. \tag{12}$$

The angle between the bodies in contact is calculated as shown in eq. (13). Where α is angle in relation to the axis of the bodies in contact, P is force in contact, E is modulus of elasticity. A_e is the area of elastic contact, given by eq. (14).

$$\alpha = \left(\frac{3E(e)PR_m}{2\pi E^*(1-e^2)}\right)^{\frac{1}{3}}. \tag{13}$$

$$\bar{A_e} = \pi ab. \tag{14}$$

2.3 Influence of GFRP rebar surface and diameter

There is an inversely proportional relation between diameter and tensile stress; the greater the diameter of the GFRP bar, the lower the tensile stress. This can occur due to the shear effect, when the stresses act on the bar surface, causing a differential movement in the interface between the fiber surface and the core of the bar [10].

Another important factor is that the Poisson's ratio effect increases along with the bar diameter. However, the pullout stress in the act of pulling decreases the section of the bar, weakening the contact between bar and concrete [11].

2.4 Adhesion of GFRP rebar

Adherence is the main characteristic to take into consideration in reinforced concrete structures with incorporation or reinforcement with GFRP bars. The adhesion behavior of these materials is a crucial factor for determining the mechanical properties [12].

The GFRP-concrete connection is ensured by a frictional force, where the acting force is transferred from the FRP polymer matrix [4, 13]. Bar surface friction affects bond quality and strength. Through the relation between the compressive strength of concrete and the shear strength of the surface, there are several types of failures that can occur due to poor adhesion between the bar and the concrete, such as: concrete shear, GFRP shear, or a combination of these factors.

3 Materials and methods

This paper was divided into two analyses: one is experimental, and the other, numerical. In the experimental program, the characterization of the materials, the molding and curing of the specimens were done according to NBR 5738. The apparatus used in the pullout tests is shown in Figure 1. A total of 18 specimens were molded, 6 with steel, 6 with GFRP and 6 with GFRP + epoxy resin. The specimens had a 15 cm edge, and the steel and GFRP rebars were 6,3 mm in diameter and 15 cm in length.

Figure 1. Pullout test experimental equipment

A numerical analysis was performed on the software Abaqus 6.14.1, the finite element used was C3D8R, a solid element with eight nodes, with three degrees of freedom in each node and reduced integral. The Abaqus contact logic is presented in Figure 2a. The friction was modeled considering the Coulomb isotropic material, for better coexistence it was necessary to alternate the friction value between 0 and 1, in addition to consider the static friction. The friction is shown in Figure 2b.

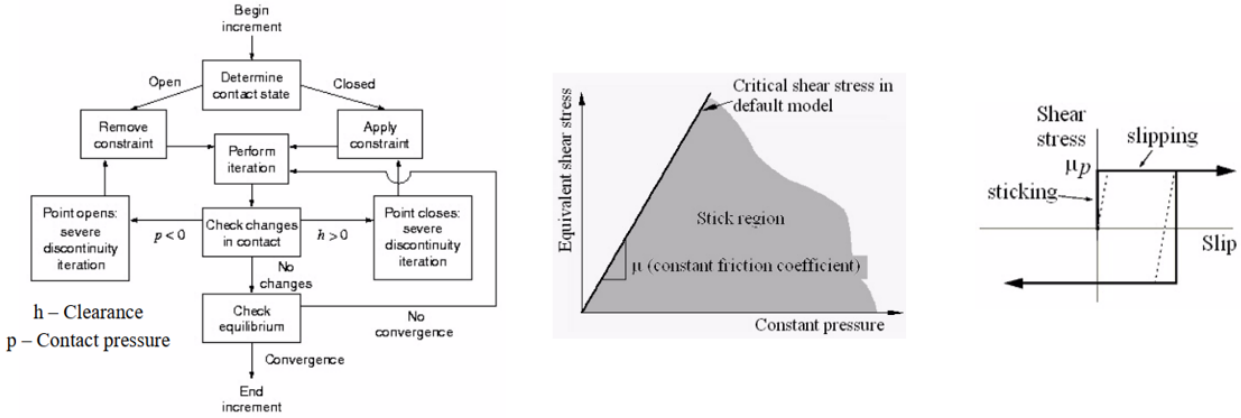

(a) Contact logic

(b) Couloumb's frictional model

Figure 2. Model of contact and friction

The steel rebars used were CA-50. The GFRP properties were: 2.109 kgf/cm^2 of maximum tensile strength, in the longitudinal direction of the fibers. Perpendicular to the fibers, the tensile strength was 492 kgf/cm^2. The tensile elasticity modulus in the longitudinal and perpendicular direction of the fibers were, respectively, 17.6000 kgf/cm^2 and 56.000 kgf/cm^2. The strength of bond between the GFRP and steel to the concrete was determined by the eq. (15).

$$\tau = \frac{F}{\pi d l_b} \tag{15}$$

In which τ is the bond strength, F is the tractive force in the test, d is the rebar diameter, l_b is the rebar length inserted in concrete. A constant load of 10,000 N was applied to the upper end of the GFRP bar and boundary

conditions corresponded to the experimental program, to ensure that surfaces in contact shared the same node. A mesh of 5 mm was assigned.

4 Results and discussions

The pullout force can be a parameter to determine the material behavior when in service. However, it is extremely important to analyze the loading and unloading process, breaking behavior - whether it is ductile or not -, stress relaxation, and plastic strains. The experimental results are shown in Figure 3. The average pullout force was slightly higher in the GFRP condition without resin, followed by the steel bar.

There was a discrepancy, so that the displacements obtained in a same series of tests had a difference of more than 6 mm. Just by analyzing the bond strength x displacement relation, the configuration that presents greater ductility is precisely the GFRP + epoxy resin model, In this configuration, low traction stress was necessary to achieve a greater displacement. However, this configuration also presents lower bond strength, as shown in Figure 3.

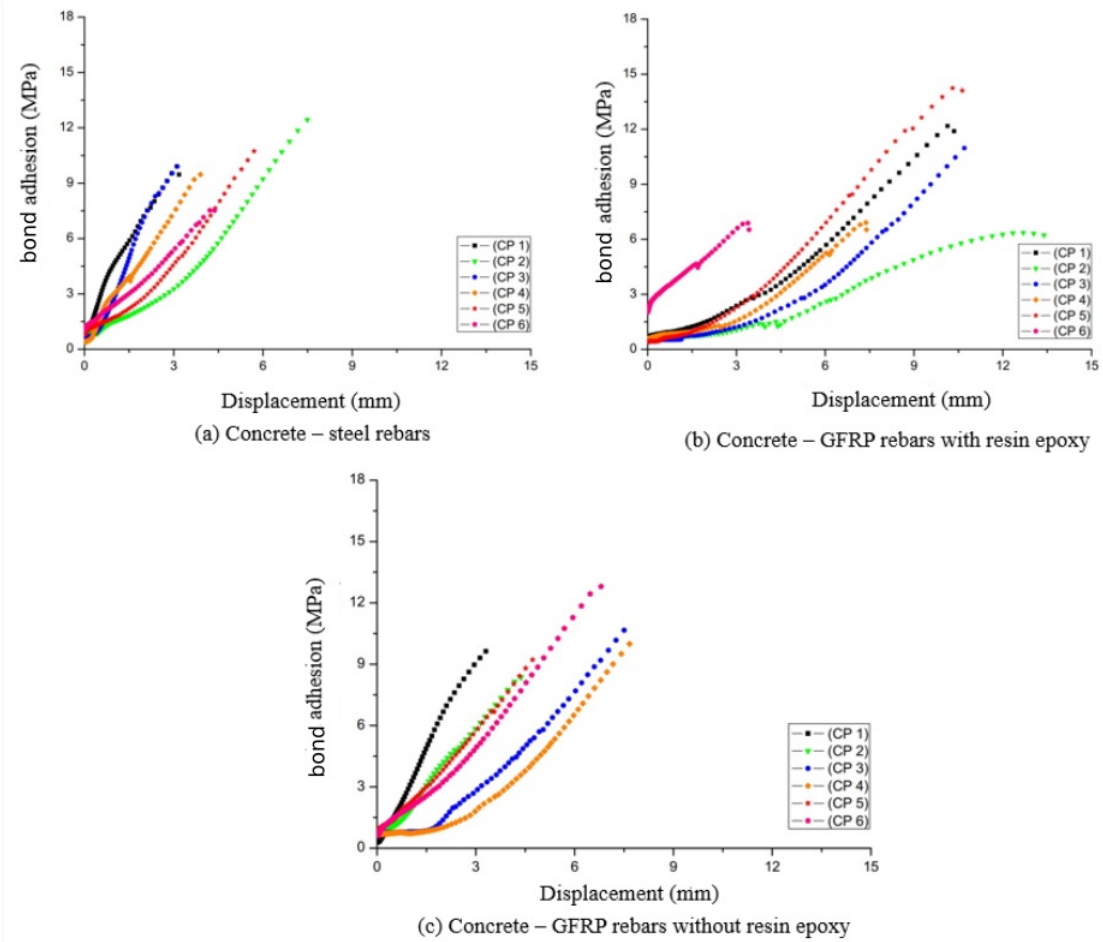

Figure 3. Relationship bond strength x displacement

The Von Mises failure criteria indicates that a certain material flows when the second invariant J_2 reaches a critical value. It can be said that there is no energy distortion when the maximum stress obtained is less than the allowable stress of the material. All the results of the numerical analysis are presented in MPa and mm, as shown in Figure 4. The material failure is precisely in the concrete-GFRP interface.

It was necessary to select only a few experimental tests to validate the numeric model. Analyzing the set above, it can be stated which is the bar where the highest stress are concentrated; the support conditions restricted the base. As shown in Figure 4, the specimen presented large displacements and, consequently, greater strain. As shown in Figures 5 and 6, it is possible to visualize the difference between numerical and experimental analyses.

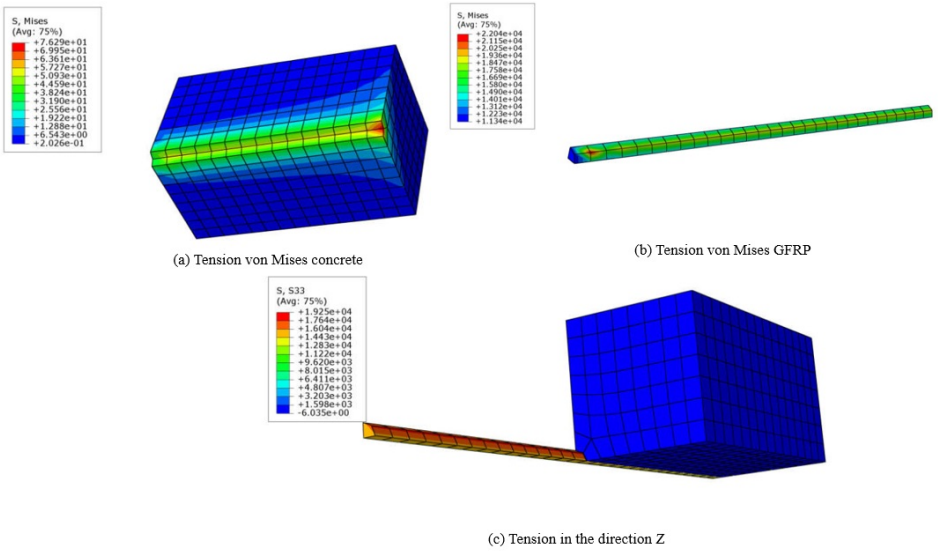

Figure 4. Results numerical pullout test

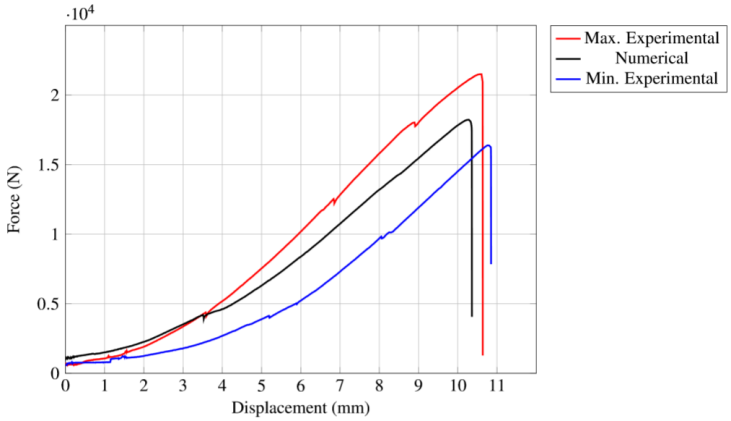

Figure 5. Comparative analysis between experimental and numerical - with resin

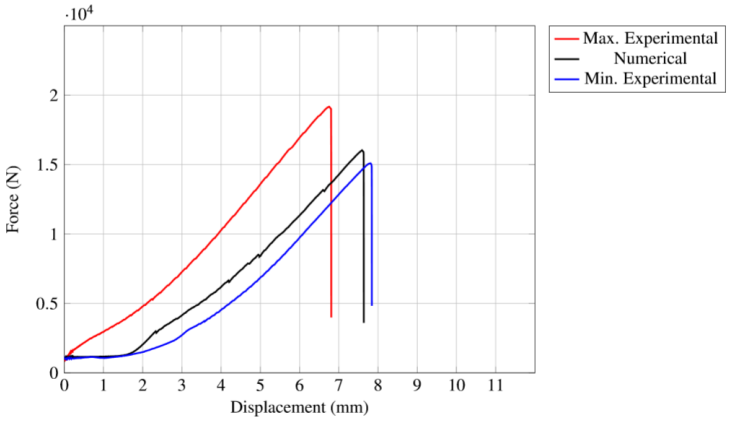

Figure 6. Comparative analysis between experimental and numerical- without resin

In Figure 3b, the CP 2, even with the lowest pullout force, obtained the largest displacement of this analysis. This was due to the properties of GFRP and fiber orientation in the matrix. When comparing the experimental program and the numerical model, the numerical analysis resides within the limits obtained in the experimental

program, showing the convergence of the model. It is noticed that the configuration with epoxy resin presented strength and displacement superior to the configuration without resin, in the order of 5% and 20%, respectively. The pullout force was 20% higher in the steel bar test when compared to the other configurations.

5 Conclusions

The pullout force of the GFRP rebar is similar to that of steel. It is well known that the application of epoxy resin does not interfere positively with the pullout force, there was a reduction of 40%, when compared to GFRP without resin and the steel. However, GFRP without resin showed a increase of 20% on pullout strength. The use of GFRP rebar is justified because it has good mechanical performance and high corrosion resistance. In Brazil, NBR 6118 considers the class of environmental aggressiveness as well as the compressive strength, useful life, and durability for concrete structural design, in these situations the GFRP performs better than steel.

Acknowledgments. To Capes for the financial support to the authors during the research. To the Materials and Civil Construction Laboratory (LMCC) of the Federal University of Ceará. To the company STRATUS FRP for supplying the GFRP rebars.

Authorship statement. The authors hereby confirm that they are the sole liable persons responsible for the authorship of this work, and that all material that has been herein included as part of the present paper is either the property (and authorship) of the authors, or has the permission of the owners to be included here.

References

[1] Rezazadeh, M., Carvelli, V., Veljkovic, A., et al., 2017a. Modeling the bond of gfrp and concrete based on a damage evolution approach. In *Fourth International Conference on Smart Monitoring, Assessment and Rehabilitation of Civil Structures (SMAR 2017)*, pp. 1–8. CHE.

[2] Fava, G., Carvelli, V., & Pisani, M. A., 2016. Remarks on bond of GFRP rebars and concrete. *Composites Part B: Engineering*, vol. 93, pp. 210–220.

[3] Wang, Y., Wu, B., Guo, Y., & Yang, H., 2017. Numerical research on the pullout failure of GFRP bolt. *Advances in Materials Science and Engineering*, vol. 2017, pp. 1–11.

[4] Imjai, T., Guadagnini, M., & Pilakoutas, K., 2017. Bend strength of FRP bars: Experimental investigation and bond modeling. *Journal of Materials in Civil Engineering*, vol. 29, n. 7, pp. 04017024.

[5] Shayanfar, M. A., Rostamian, M., Ghanooni-Bagha, M., Tajban, A., & Nemati, S., 2018. Evaluating the plasticity of concrete beam-column connections reinforced with FRP composite rebars. *Engineering Solid Mechanics*, pp. 331–340.

[6] Arani, K. S., Zandi, Y., Pham, B. T., Mu'azu, M., Katebi, J., Mohammadhassani, M., Khalafi, S., Mohamad, E. T., Wakil, K., & Khorami, M., 2019. Computational optimized finite element modelling of mechanical interaction of concrete with fiber reinforced polymer.

[7] Chen, Z., Que, M., Zheng, L., Li, X., & Sun, Y., 2020. Effect of mortar constraint conditions on pullout behavior of GFRP soil nails. *Advances in Materials Science and Engineering*, vol. 2020, pp. 1–11.

[8] Prakash, C. & Sekar, K. S. V., 2018. 3d finite element analysis of slot milling of unidirectional glass fiber reinforced polymer composites. *Journal of the Brazilian Society of Mechanical Sciences and Engineering*, vol. 40, n. 6.

[9] Rezazadeh, M., Carvelli, V., & Veljkovic, A., 2017b. Modelling bond of GFRP rebar and concrete. *Construction and Building Materials*, vol. 153, pp. 102–116.

[10] Kusnadi, Djamaluddin, R., Muhiddin, B., & Irmawaty, R., 2020. The bonding strength of GFRP bars embedded within concrete under direct pull-out test. *IOP Conference Series: Earth and Environmental Science*, vol. 419, pp. 012062.

[11] Lin, J.-P. & Wu, Y.-F., 2016. Numerical analysis of interfacial bond behavior of externally bonded FRP-to-concrete joints. *Journal of Composites for Construction*, vol. 20, n. 5, pp. 04016028.

[12] Gooranorimi, O., Suaris, W., & Nanni, A., 2017. A model for the bond-slip of a GFRP bar in concrete. *Engineering Structures*, vol. 146, pp. 34–42.

[13] Hajiloo, H. & Green, M. F., 2019. GFRP reinforced concrete slabs in fire: Finite element modelling. *Engineering Structures*, vol. 183, pp. 1109–1120.